Icarus 355 (2021) 114110

Contents lists available at ScienceDirect

Icarus

journal homepage: www.elsevier.com/locate/icarus

Research Paper

Suggestion that recent ($\leq$ 3 Ga) flux of kilometer and larger impactors in the Earth-Moon system has not been constant

Michelle R. Kirchoff *, Simone Marchi, William F. Bottke, Clark R. Chapman, Brian Enke

Southwest Research Institute, Boulder, CO 80302, USA

ARTICLE INFO

Keywords:
Cratering
Lunar Chronology
Moon
Surface
Asteroids
Dynamics
Impact flux

ABSTRACT

Lunar impact crater chronologies have been developed by combining carefully measured crater densities of lunar terrains with radiometric ages provided by returned samples. However, due to the sparse coverage of the samples during the last three billion years, this part of the chronologies is not well constrained. Lunar crater chronologies generally assume that the bombardment rate has been relatively constant during this epoch for all impactor sizes. Nevertheless, evidence has been gathering that this may not be the case for impactors larger than several hundred meters; however, there may be biases related to some of this evidence. The break-up of large asteroids in the Main Asteroid Belt to make asteroid families could be a source of a changing impact flux in the Earth-Moon system, especially when the families form near strong orbital resonances with the gas giants. In order to further explore the state of the impact flux from today to three billion years ago for impactors larger than ~5 km, we calculate crater retention model ages of 43 lunar craters 50 km and larger in diameter (D). Selected craters were initially suggested by United States Geological Survey geological maps of the Moon and Wilhems (1987) to have formed during the Copernican and Eratosthenian. We use the density of small (D < a few km) craters superposed on their floors, along with Model Production Function (MPF) lunar chronology (Marchi et al., 2009). For this purpose, we assume that the smaller impactors forming the superposed craters follow a constant flux as indicated by the MPF and supported by models of the dynamical evolution of the impactor population. We use the model ages as a proxy for the impact flux of larger impactors and test whether their distribution in time is consistent with a constant flux using two statistical analyses. Our results suggest that the flux of these larger impactors could be variable during the last three billion years, with hints of a relative increase in flux occurring ~2 billion years ago and a decrease in flux ~1 billion years ago. Thus, our results support the evidence that the impact flux has varied on the Moon for impactors over a few kilometers in diameter.

1. Introduction

Absolute cratering chronologies for the Moon have been developed as a outcome of human and robotic sample return missions (e.g., Hartmann et al., 1981; Le Feuvre and Wieczorek, 2011; Marchi et al., 2009; Neukum et al., 2001; Neukum and Ivanov, 1994; Robbins, 2014). These chronologies pair the crater spatial densities from known regions to the radiometric ages of the returned samples (e.g., Stöffler et al., 2006; Stöffler and Ryder, 2001). The problem is that because locations and samples are limited, there are still many unknowns about the chronology, especially in recent epochs, from about three billion years ago until today. In general, the published lunar chronologies assume that the flux has been relatively constant during this time period for all impactors regardless of size. Evidence has been developing, however, that this may not be the case.

Relative increases in crater production for relatively short time periods of about a few hundred million years ("spikes") in the last few billion years for the Earth-Moon system have been noticed in a variety of data sets. We start by listing this evidence, then discuss the issues.

First, potential spikes in the production of lunar impact glasses have been observed in various Apollo samples at ~0.5, 0.8, 1.5, and 2.5 Ga (Culler et al., 2000; Hui et al., 2009; Levine et al., 2005; Muller et al., 2001; Norman et al., 2012; Zellner et al., 2009; Zellner and Delano, 2015). Second, similar spikes are indicated by the increased number of L-chondrite fossilized meteorites found on Earth at ~0.5 and 0.8 Ga (Schmitz et al., 2003). Third, the radiometric ages of craters on Earth may show evidence for an increase in the flux within the last few hundreds of millions of years and a potential increase around 2 Ga (Grieve,

* Corresponding author.
E-mail address: kirchoff@boulder.swri.edu (M.R. Kirchoff).

https://doi.org/10.1016/j.icarus.2020.114110
Received 29 August 2019; Received in revised form 11 September 2020; Accepted 11 September 2020
Available online 18 September 2020

1984; Grieve and Shoemaker, 1994). The former was recently quantified by Mazrouei et al. (2019), who argued that a factor of 2–3 increase in the production rate of diameter (D) > 10–20 km craters on the Earth and Moon started ~290 Ma. In their method, they used the thermophysical characteristics of lunar impact ejecta as measured with the Diviner thermal radiometer on NASA's Lunar Reconnaissance Orbiter (LRO) to date craters across the Moon younger than 1 Ga. Finally, previous efforts to understand the absolute crater model ages of large lunar craters using smaller craters superposed on them has shown that occasional short-lived increases in the impact flux have taken place; some events also have ages similar to those discussed above (Baldwin, 1985; McEwen et al., 1993). Additional support for a recent spike at ~1 Ga using this methodology of dating the formation ages of larger craters using smaller superposed craters comes from Mars (Lagain et al., 2020), implying changes in flux throughout the inner solar system.

On the "con" side, we caution that recent works have argued that the young spikes indicated by Apollo glasses could be due to thermal strain breaking up glasses (Zellner and Delano, 2015) and/or sampling and other biases (Huang et al., 2018; Hui et al., 2009). Optical maturity studies of lunar rayed craters also counter-indicate an increase of impact flux at 800 Ma (Grier et al., 2001; Grier and McEwen, 2001). Finally, work by Guinness and Arvidson (1977) argued for a constant flux for craters between 0.1 and 1 km in diameter over the last 3.3 Ga given the similarity in the crater size-frequency distribution shapes for terrains examined in this time frame.

Short or long-term relative decreases from average in the impact flux ("lulls") in the last few billion years have also been potentially indicated. One such lull was suggested by Mazrouei et al. (2019), who argued from their lunar crater ages that the impact flux was distinctly lower between ~300–1000 Ma. They argued that a lower impact flux is also seen in terrestrial craters formed on cratons between 300 and 650 Ma. Others believe this terrestrial crater deficit might be a result of erosion and crater degradation (see Grieve, 1984), though this would not explain the relatively intact nature of kimberlite pipes found in the same locations as terrestrial craters (see also Keller et al., 2019). Long-term lulls (or declines in the impact rate since ~3 Ga) have been suggested based upon slower than expected crater degradation rates (Craddock and Howard, 2000), along with ages of lunar impact melts (in lunar meteorites) and lunar glasses (excluding the indicated spikes discussed above) (Hartmann et al., 2007). A long-term lull between 1 and 2 Ga was also indicated for Mars using superposed crater densities on larger craters by Lagain et al. (2020).

Observations and simulations have shown that the break-up of large asteroids by impacts to produce families is not uncommon (Bottke et al., 2007; Gladman et al., 1997; Masiero et al., 2015; Nesvorný et al., 2002, 2015; Vokrouhlický et al., 2017; Zappalà et al., 1998). Observations of the dynamical properties of the families can provide the approximate time of their formation (Bottke et al., 2006; Nesvorný et al., 2002, 2015). Furthermore, simulations have shown when these break-ups occur near resonances they can become sources for increased delivery of objects to impact the Earth-Moon system (e.g., Bottke et al., 2007; Vokrouhlický et al., 2017; Fig. 1). Observations of impact events timing for the parent bodies of meteorites support this idea (e.g., Nesvorný et al., 2009).

So far the size of impactors involved in the possible observed spikes or lulls and produced by the asteroid break-ups has not been specified. The observations discussed above potentially cover a wide range of impactor sizes from meters (fossil meteorites and impact glasses) to several tens of kilometers (large craters and impact melts). Thus, increases or decreases in the number of impactors created and delivered to the Earth-Moon system could be occurring at a wide range of sizes at different times or i.e., the size-frequency distribution of the impactors changes shape, if all observations are accepted equally. Furthermore, simulations indicate the rate of increased delivery over the background rate is potentially different for different impactor sizes. Small impactors, less than a few hundred meters or so, do not appear to increase much over their background except for very short time periods (Guinness and Arvidson, 1977; Nesvorný et al., 2009), while larger impactors, appear to show increases lasting a few hundreds of millions of years over the background flux at these sizes (Bottke et al., 2007; Mazrouei et al., 2019; Fig. 1). This would imply that at certain sizes we would see an increase

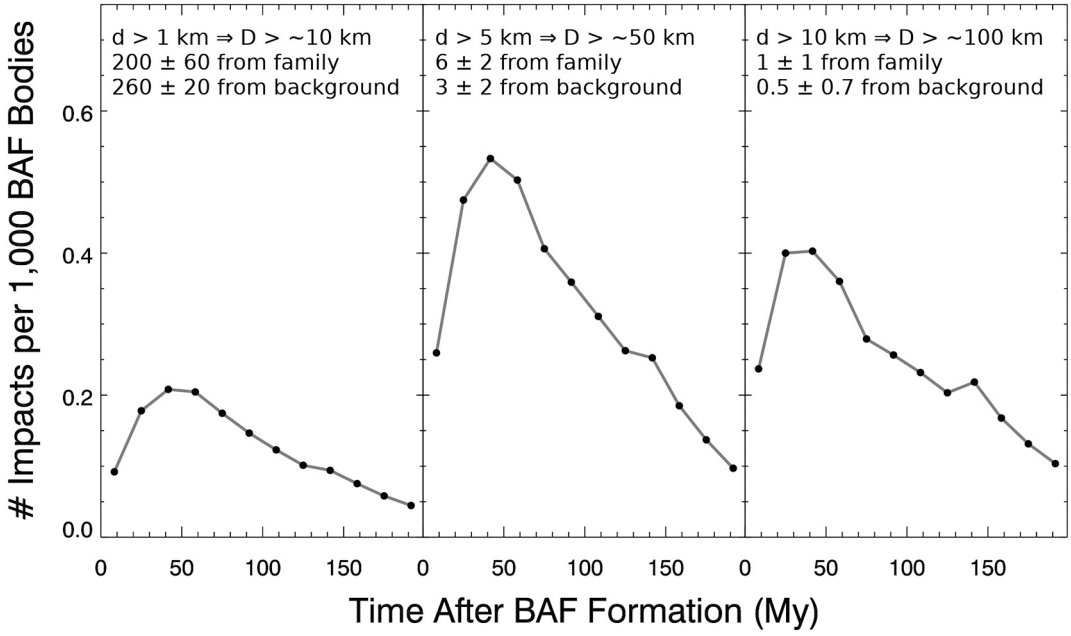

Fig. 1. Simulation results of impacts in the Earth-Moon system from the Baptistina asteroid family (BAF) by Bottke et al. (2007). Each panel is for a different sized impactor (d) from smaller to larger impactors going left to right. Using simple scaling (x10; Marchi et al. (2009)) the approximate crater diameter (D) formed on the Moon is also shown. Based upon these simulation results Bottke et al. (2007) predict the number of impacts shown for each impactor diameter from the family and the background source of impactors. Note that fewer D > ~10 km craters are expected from the family than from the background impactors, while more D > ~50 and 100 km craters are expected from the family than the background. This would result in a 'spike' in impacts over an ~100 Myr timespan for larger craters, while D < ~10 km would remain relatively constant. Figure modified from Bottke et al. (2007).

in crater production on the Earth and Moon at certain times.

We use modern versions of the techniques used by Baldwin and McEwen to derive the absolute crater model ages and flux of large lunar craters. We measure small craters (D ~ 0.01–5 km, likely made by projectiles that are sub-meter to a few hundred meters) superposed on their floors, since floors appear to provide a more reliable estimation of the crater distribution than counts on the ejecta blankets for the Moon (Plescia, 2012; Plescia and Robinson, 2011; Zanetti et al., 2017). Then, we use the Model Production Function (MPF; Marchi et al., 2009) lunar chronology to fit the crater size-frequency distributions and derived absolute model ages of the large craters. We assume that the flux of the smaller and larger craters are disconnected, with the small craters having the constant flux as expected by the MPF (see Guinness and Arvidson, 1977 and supplemental materials in Mazrouei et al., 2019). As described above, this may be theoretically expected if asteroid families are the cause of changes in flux, as simulations indicate that the large impactors from families do increase above background, while the small ones do not (Bottke et al., 2007; Fig. 1). In Section 2, we present our methods, including discussion of the sources of uncertainties in the absolute model ages, such as secondary craters. In Section 3, we present the ages and statistical analyses of the implied flux. Finally, in Section 4, we discuss the implications for any observed variations from a constant flux and comparisons with known families and other data sets indicating variability in the flux.

2. Methods

Because we are interested in the crater flux during the Copernican and Eratosthenian eras (~0–3.2 Ga; Stöffler and Ryder, 2001), we analyze craters initially identified as potentially forming in those epochs by the United States Geological Survey (USGS) geological maps of the Moon from the 1970s (e.g., Wilhelms and McCauley, 1971) and/or Wilhelms (1987). These researchers typically used the morphology of the craters to determine which era they formed in, such as occurrence and brightness of ejecta and erosional state of the crater rim and peak; and they did not always agree. For example, we have a few craters labeled by the USGS maps as forming in the L. Imbrian (Fabricus, Leuschner, and Werner; see our Table 2), as Wilhelms identified them as forming in the Eratosthenian (see Supplemental Material). We note that by not including all craters labeled as formed in the Imbrian by both these earlier data sets, we may have missed some craters that could have crater retention model ages consistent with possible formation in the Copernican or Eratosthenian. However, we expect this number to be low, as typically our crater retention model ages indicate the same epoch or older, instead of younger ages (Table 2). In fact, we only observe *one* crater with a crater retention model age less than its morphological age as determined by either earlier classification (Ohm, Table 2). Furthermore, in our earlier study (Kirchoff et al., 2013), where we included some initially labeled Imbrian craters, we found *none* of these were younger than their initially predicted ages. Thus, given a maximum rate of ~2% that could be younger using our methods, we would only expect up to a couple of additional craters, which would not likely change the answer significantly. An example is Tsiokolvskiy, which we do include, because recent work has indicated it may indeed be Eratosthenian in formation age (Greenhagen et al., 2016). However, evidence has been scarce in the literature for a scenario similar to Tsiokolvskiy for other large lunar craters. We then chose to examine craters with diameter (D) $\geq$ 50 km, since the impactor diameter expected to produce this size crater (~2 km) is plausibly well above the impactor size where the flux may switch from constant to non-constant (e.g., Fig. 1; Bottke et al., 2007; Mazrouei et al., 2019). These criteria resulted in 45 craters with D $\geq$ 50 km (Table 1; Fig. 2).

Because all but two of the craters (Copernicus and Tycho) do not have radiometric ages from samples that are potentially associated with their formation age, we are required to use a lunar crater chronology to estimate their absolute model ages. For this purpose we measure the density of smaller craters superposed on their floors (which we abbreviate SSC for small, superposed craters) (e.g., Fig. 3). We use both the LROC Wide Angle Camera (WAC) global mosaic at a pixel scale of 100 m/pixel at the equator and LROC Narrow Angle Camera (NAC) images at pixel scales of 0.5–1 m/pixel. The NAC images are primarily needed for smaller and younger craters to obtain enough SSCs to reduce uncertainties on the crater distributions. We use JMARS (http://jmars.asu.edu/) to view the WAC global mosaic and find NAC images where needed.

There are two craters – Hercules and Tsiolkovskiy – which have had their floors covered by maria, making it difficult to include them using our methods. We considered instead counting their ejecta blankets, but this would introduce a difference in ages due to differing terrain properties (e.g., Kirchoff and Marchi, 2019; Marchi et al., 2011; van der Bogert et al., 2017). This could be theoretically corrected for using the MPF (e.g., Marchi et al., 2009); however, the correction to use to get the most reliable age is uncertain (e.g., Kirchoff and Marchi, 2019). Therefore, we decided not to introduce this additional uncertainty using a different methodology. Nevertheless, we did want to understand the effect of including these craters, so we measured superposed craters on the mare (which should have similar material properties to crater floors) to get a minimum age for these craters and then assumed the maximum age is the maximum for the Eratosthenian (3.2 Ga). For Tsiolkovskiy,

Table 1
List of large craters analyzed.

#	Name	Location	Diameter (km)
1	Kirkwood	68°N, 157°W	68
2	Jackson	22°N, 163°W	71
3	Morse	22°N, 175°W	73
4	Finsen	42°S, 178°W	73
5	Vavilov	1°S, 139°W	99
6	Robertson	21°N, 105°W	90
7	Ohm	18°N, 114°W	62
8	Leuschner	2°N, 109°W	50
9	Maunder	15°S, 94°W	54
10	Hausen	65°S, 89°W	163
11	Carpenter	70°N, 51°W	59
12	Pythagoras	64°N, 63°W	145
13	Cavalierius	5°N, 67°W	59
14	Zucchius	61°S, 51°W	63
15	Philolaus	72°N, 33°W	71
16	Copernicus	10°N, 20°W	96
17	Bullialdus	21°S, 22°W	61
18	Hainzel A	40°S, 34°W	56
19	Anaxagoras	74°N, 10°W	52
20	Eratosthenes	15°N, 11°W	59
21	Tycho	43°S, 11°W	86
22	Moretus	71°S, 6°W	115
23	Aristillus	34°N, 1°E	54
24	Werner	28°S, 3°E	71
25	Scoresby	78°N, 14°E	55
26	Aristoteles	50°N, 17°E	88
27	Eudoxus	44°N, 16°E	70
28	Hercules	47°N, 39°E	68
29	Theophilus	12°S, 26°E	99
30	Fabricus	43°S, 42°E	79
31	Geminus	34°N, 57°E	82
32	Taruntius	6°N, 47°E	57
33	Langrenus	9°S, 61°E	132
34	Stevinus	33°S, 54°E	72
35	Hayn	64°N, 84°E	86
36	Plutarch	24°N, 79°E	70
37	Hamilton	43°S, 84°E	58
38	Moiseev	10°N, 103°E	62
39	Olcott	21°N, 118°E	80
40	King	5°N, 121°E	76
41	Tsiolkovskiy	20°S, 129°E	184
42	Ricco	75°N, 177°E	66
43	Sharonov	12°N, 173°E	75
44	O'Day	30°S, 157°E	70
45	Birkeland	30°S, 174°E	82

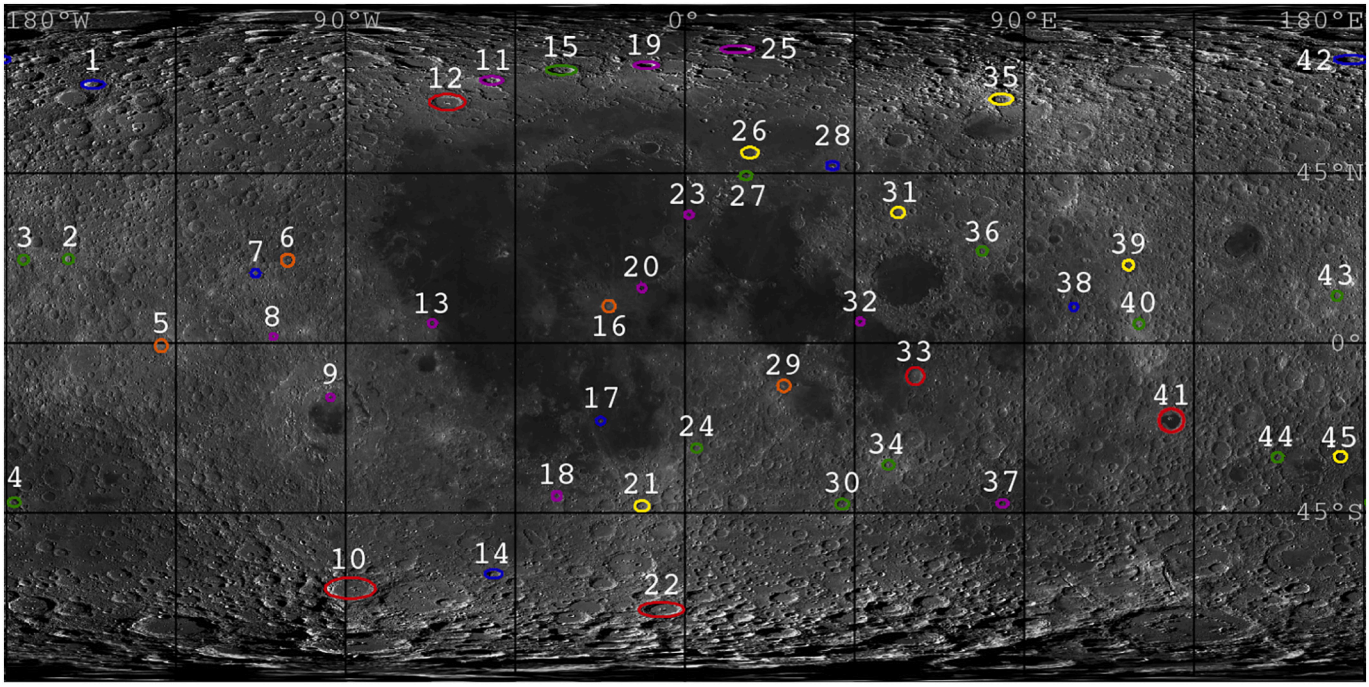

Fig. 2. Locations of study craters as indicated by colored circles. Numbers correspond to the numbers given in Table 1. Sizes are indicated by the colors with red for D ≥ 100 km, orange for D = 90–99 km, yellow for D = 80–89 km, green for D = 70–79 km, blue for D = 60–69 km, and purple for D = 50–59 km. (For interpretation of the references to color in this figure legend, the reader is referred to the web version of this article.)

there may be small areas of the original floor left (see Supplemental Fig. S40), so we measured superposed craters on these as well to get additional constraints on this crater's formation age.

We use the JMARS 3-point crater tool to measure SSCs once identified. This tool provides the diameter of the SSC, along with its center latitude and longitude. We also classify the SSCs with a degradation state and if they are an obvious secondary crater (e.g., Fig. 3). Degradation state is on a scale of 1–4 with 1 representing the freshest craters with sharp rims, deep cavities, and no visible superposed craters (e.g., Fig. 3, red circles). Classes 2 and 3 have more eroded rims and cavities that are partially filled (e.g., yellow and green circles, respectively in Fig. 3), with Class 2 craters having sharper rims and deeper bowls than Class 3. Class 4 craters are the most eroded, sometimes with no identifiable rim and little depth (e.g., Fig. 3, blue circles). Crater depth is subjectively determined by shadows. Secondary craters are those that form from the fast, blocky ejecta of a larger primary crater. Obvious secondary craters (OSCs) then are defined here as those secondary craters that form in chains and clusters, and may have a distinctive herringbone pattern (e.g., Fig. 3, pink circles; e.g., Oberbeck and Morrison, 1974). We do not classify lone elliptical craters as OSCs as they may be elliptical primaries. For further details on classifications see Kirchoff et al. (2013).

Once we have compiled the SSCs for each large crater, we analyze the SSC size-frequency distributions (SFDs). We use the cumulative, differential, and relative (R) formats (Crat. Anal. Tech. Work. Group, 1979) as they each have something unique to offer for the analyses. The cumulative distribution is used to derive the relative and absolute model ages of the large craters (e.g.. Figs. 3, 4). The differential distribution is used to compare the presumed primary SSC SFD with the crater SFD for the OSCs, along with computing the differential slope for the SSC and OSC SFDs (e.g., Fig. 4). The R-plot is used to compare how the various crater degradation classes contribute to the SSC SFD and the overall shape of the SSC SFD (e.g., Fig. 4).

We use the new, more statistically robust techniques described in Robbins et al. (2018) to compute all SSC SFDs (e.g., Figs. 3, 4). These techniques use a kernel density estimator (KDE) to compute the crater SFDs and bootstrap to compute the associated uncertainties. We also use the recommended minimum likelihood estimator (MLE) technique for computing the differential slope. The advantages of these techniques is that they include more uncertainties associated with crater measurements than traditional techniques. First, the KDE allows us to include the uncertainty on the diameter measurement into the SFD (Robbins et al., 2018). Second, bootstrap uncertainties are derived directly from the data without the need to assume a structure to the data that may not be correct (e.g., Poisson). They have also been expanded to represent the 99th percentile (equivalent to 3σ for a Gaussian; in the differential and cumulative plots the traditional 2σ equivalents are also shown by the lighter lines within the shaded areas), thus potentially incorporating more sources of error. Finally, MLE also relies directly on the data rather than assuming it has a structure and has less error and restrictions (e.g., requiring a certain number of points) associated with the fit to the data. We show traditional versions of each of the cumulative crater SFDs represented by squares with error bars to demonstrate that the new technique corresponds to traditional ones well while providing more statistically robust information. Plots similar to Fig. 4 are given for all craters in Supplementary Material (excluding representation of traditional techniques).

Absolute ages and their uncertainties are estimated using the Model Production Function for the Moon (MPF; Marchi et al., 2009) to a precision of 0.1 Ga (e.g., Fig. 3; we suggest this is the minimum precision for any lunar crater chronology; see e.g., Kirchoff et al., 2013). This chronology is able to incorporate the different distributions for both Near Earth Objects (NEO) and Main Belt Asteroids, along with the effect of terrain strength on the formation of craters with diameters less than about a few hundred meters, when computing the shape of the crater production function. Based upon our preliminary understanding of relevant impactors, terrain properties, and sizes of SSCs (D > 10 m), we start with using the distribution for NEOs and the gravity-regime scaling law for competent rock from Melosh (1989); eqs. 7.8.4, target density = 2.8 g/cm^3, projectile density = 2.6 g/cm^3, and impact velocity distribution from fig. 1 in Marchi et al., 2009; converted to final diameters using standard relationships and simple-to-complex transition diameter of 18 km, e.g., Marchi et al., 2009). We find that this production function

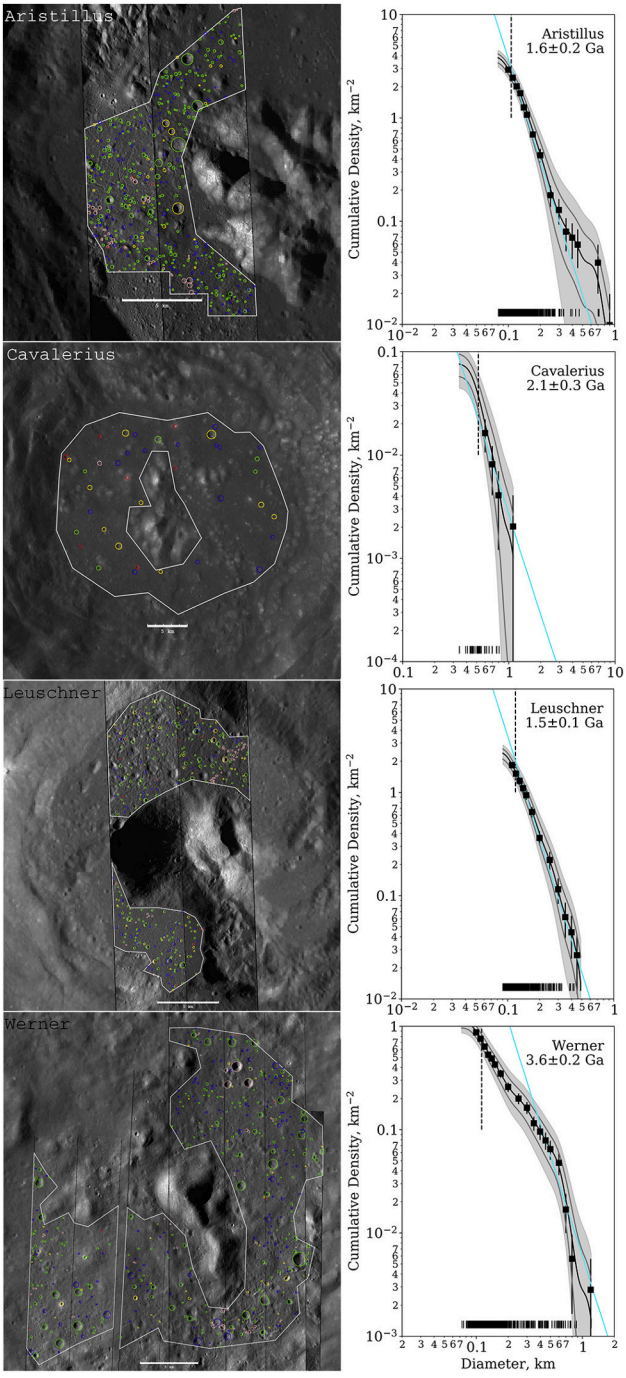

Fig. 3. Examples of crater measurements, cumulative SFDs, and fitting with the MPF. Left column shows the crater measurements and NAC images, if used, superposed on the WAC mosaic. Colored circles represent the SSCs measured and their classification. Red are class 1 craters, yellow for class 2, green for class 3, and blue for class 4. Pink circles denote the OSCs. Right column shows the cumulative SSC SFDs in both the new KDE format (black/gray lines and shaded areas) and traditional binned format (black squares and error bars). The solid cyan line is the best MPF to the data and the computed age is indicated in the upper right. The vertical, dashed black line indicates the completeness diameter (below which data are incomplete) and small vertical lines at bottom of plot indicate diameter of each SSC (i.e., rug plot). (a) Aristoteles. Example of data fit well by the MPF for small craters, but not large. (b) Cavalerius. Data only collected from WAC mosaic, so data are reduced; however, SFD is fit well by the MPF. (c) Leuschner. Example of data fit well by the MPF over complete diameter range. (d) Werner. Example of large craters fit well by the MPF, but not small. (For interpretation of the references to color in this figure legend, the reader is referred to the web version of this article.)

generally fits our data well, and thus have not explored other possible production functions with different scaling laws. However, there is some variation in the fits as shown in Fig. 3. For Aristillus and Leuschner we see examples of "good" fits to data gathered from NAC images. A "good" qualitative assessment implies most or all of the cumulative crater SFD was fit well by the MPF. The SFD for Aristillus does not have a perfect fit because the SFD of the larger craters has a more shallow slope than the MPF. This "v-shape" (called such due to its appearance in a R-plot) has been observed before (Hartmann, 1995; Kirchoff et al., 2013) and may be a characteristic of the impactor population, but is more likely here due to poor statistics for these largest SSCs in a small count area (e.g., Warner et al., 2015). For Cavelerius and Werner, we see examples of "adequate" fits to data. The qualitative definition of an "adequate" fit is that either part of the SSC SFD was fit well, but another part is not (e.g., Werner), or that there are fewer points that are fit well (e.g., Cavelerius). Cavelerius superposed counts are only compiled from the WAC mosaic (SSC diameters are restricted to be ≥500 m to assure completeness). Due to the low density of craters, there are not many data points to fit and uncertainties are large; nevertheless, the MPF actually fits the few data points well. For some of the large craters, however, this was not the case and data only from the WAC mosaic resulted in a poor fit (e.g., D ≥ 500 m craters for Aristillus in Fig. 3). Thus, for these we used NAC images to expand the SSC SFDs to smaller diameters to see if the fit could be improved. This helped improve the fits and estimated absolute model ages for several craters, as exemplified with Aristillus (Fig. 3; see also Supplemental Fig. S2). However, we also observed some cases where the additional data did not help, such as Werner (Fig. 3). This is because the shape (or slope) of small lunar craters with diameters less than a couple hundred meters can vary due to several reasons (for additional review see Williams et al., 2017): 1) erosion of small craters (e.g., Fassett and Thomson, 2014), 2) crater saturation (e.g., Hirabayashi et al., 2017), 3) unrecognized, isolated secondaries (e.g., Bierhaus et al., 2018), and/or 4) effect of craters forming in the strength regime (e.g., Marchi et al., 2009). Reason #4 is not likely for most of our SSC SFDs because this effect does not cause such a dramatic change in slope – the turnover is usually more subtle (Kirchoff and Marchi, 2019; Marchi et al., 2009). Therefore, it is likely due to either all or one of the other reasons, and this part of the SFD should not be fit as we have done for Werner (Fig. 3) and other SSC SFDs affected in this way (Supplemental Figs. S9, S31, S35).

Once absolute model ages are computed, we use the large crater morphology to determine if the ages are likely formation ages of these craters. In general, the relative youth of these craters and their generally preserved morphologies indicate we are likely obtaining their formation ages with the SSCs observed on their floors (i.e., the floors have not been significantly resurfaced). The exceptions are Hercules and Tsiolkovskiy, which have their floors apparently covered by mare. As we have discussed above, we have estimated minimum and maximum ages for these craters with the formation age likely somewhere in between. The formation ages can then be used as a proxy for impact flux for these sized craters and associated impactor sizes (roughly 2–10 km).

To determine if the impact flux has been constant or variable in the last 3 Ga for these sized impactors, we use two Monte Carlo-type analyses to determine how frequently the observed distribution of craters' ages would occur for a constant flux. First, we draw ages for 0.1 Ga intervals to correspond to our model age precision for the number of craters observed for each diameter range (≥100 km, ≥90 km, ≥80 km, ≥70 km, ≥60 km, and ≥ 50 km) *only* with ages ≤3 Ga (e.g., seven ages for D ≥ 80 km craters) from the constant portion of the MPF lunar chronology (Marchi et al., 2009). Once an age from 0.1 to 3 Ga is randomly assigned, we give it an uncertainty randomly selected from the range we observe (0.1–0.7; see Table 2). We assume there is no size dependence (i.e., production function) in the formation of craters for the flux – all sizes have an equal probability of forming. From these sets, we create 100 individual summed kernel density functions (a.k.a., an ideogram), where the kernel has a Gaussian shape centered at the age

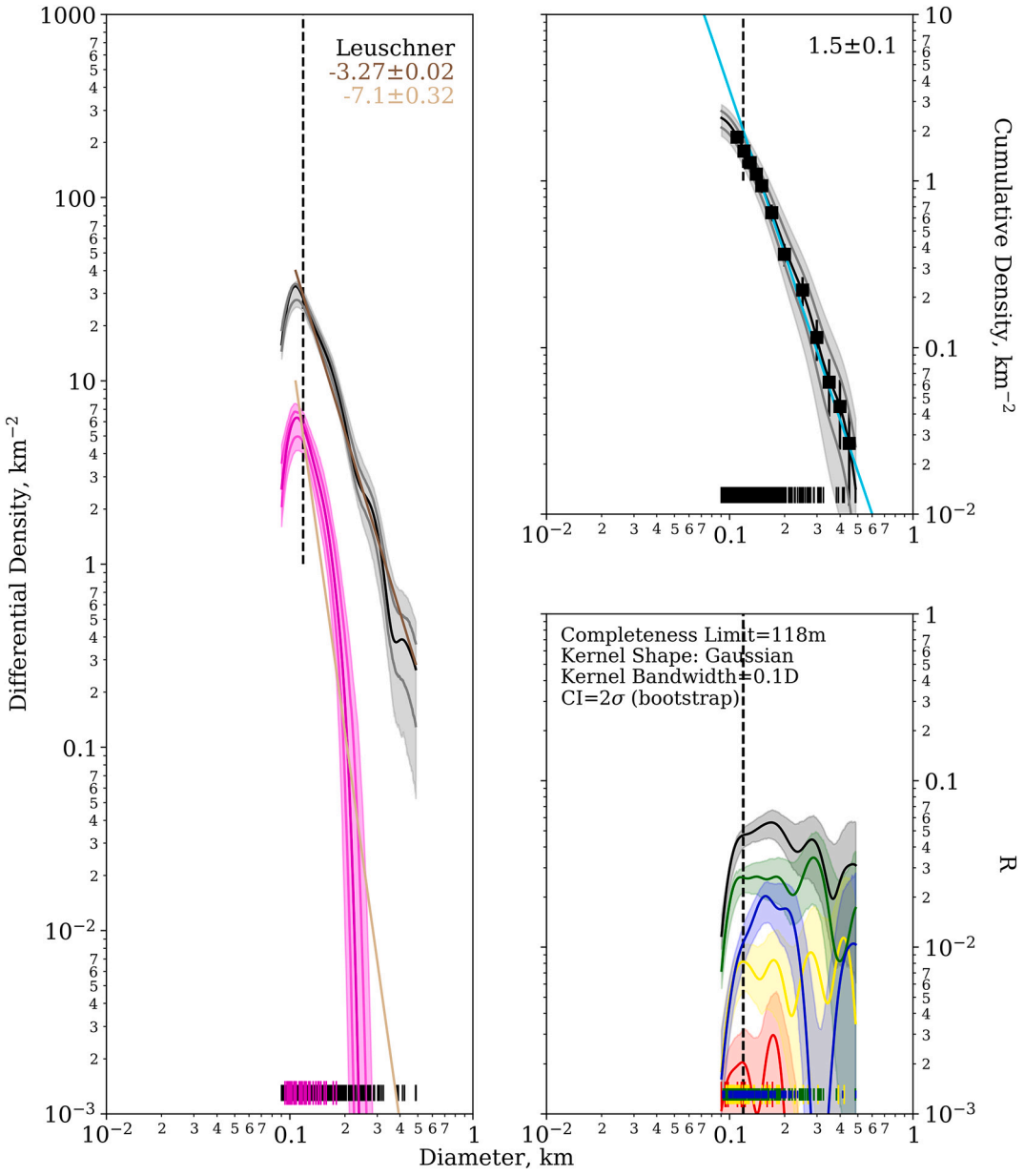

Fig. 4. Example of generating and analyses of the different crater SFD formats. Solid lines with shaded areas represent the KDE and bootstrap versions of the crater SFDs and their uncertainties. Squares and error bars represent the traditional version of the cumulative crater SFD and its uncertainty for comparison. Left plot: differential crater SFDs of all SSCs excluding OSCs (black/gray) and OSCs (pink), along with computed slopes in brown and tan respectively. Upper right plot: cumulative crater SFD of all SSCs excluding OSCs with best MPF fit (cyan line) and computed model age. Lower right plot: relative crater SFDs of all SSCs excluding OSCs (black/gray), class 1 SSCs (red), class 2 SSCs (yellow), class 3 SSCs (green), and class 4 SSCs (blue). In all plots the vertical dashed line indicates the completeness diameter with value given in the relative plot along with other information related to computing the KDE and bootstrap uncertainties. All plots also display a "rug plot" of the crater diameters measured (small vertical lines at bottom of plots). (For interpretation of the references to color in this figure legend, the reader is referred to the web version of this article.)

and a width derived from the randomly selected uncertainty (uses the norm function from the Python SciPy package). We also create an ideogram for the observed ages and their uncertainties computed from the MPF fit to the data for each diameter range (see e.g., Fig. 6, dashed gray lines; while we use published radiometric ages for Copernicus and Tycho, we continue to use our 0.1 Ga minimum uncertainty for these tests). Using these continuous functions, we can perform a Kolmogorov-Smirnov test (K–S test; e.g., Wall and Jenkins, 2003) to determine if the observed data and drawn data come from the same (constant) distribution. If we observe any distributions for a diameter range that are different at a $\geq$ 95% significance level, then we conclude the observed distribution of ages with their uncertainties is not likely derived from a constant flux. Note that due to the small numbers of craters, the distribution of D $\geq$ 100 and 90 craters could not be tested with this technique.

Second, to test the distributions with few ages less than 3 Ga (D $\geq$ 90 and 100 km), and determine when and what type of deviation from constant flux may have occurred, we modify the first analysis above. We now randomly draw crater ages with a precision of 0.1 Ga from the full MPF lunar chronology (Marchi et al., 2009), which assumes a constant flux from now until 3 Ga and then exponential for >3 Ga. However, we have modified the exponential to decrease to zero craters by 4 Ga (Fig. 5). This modification is done for two reasons: 1) our interest is for craters that have formed from $\leq$3 Ga, so we do not expect to analyze many craters older than ~3.8 Ga, and 2) SSCs less than a kilometer or so

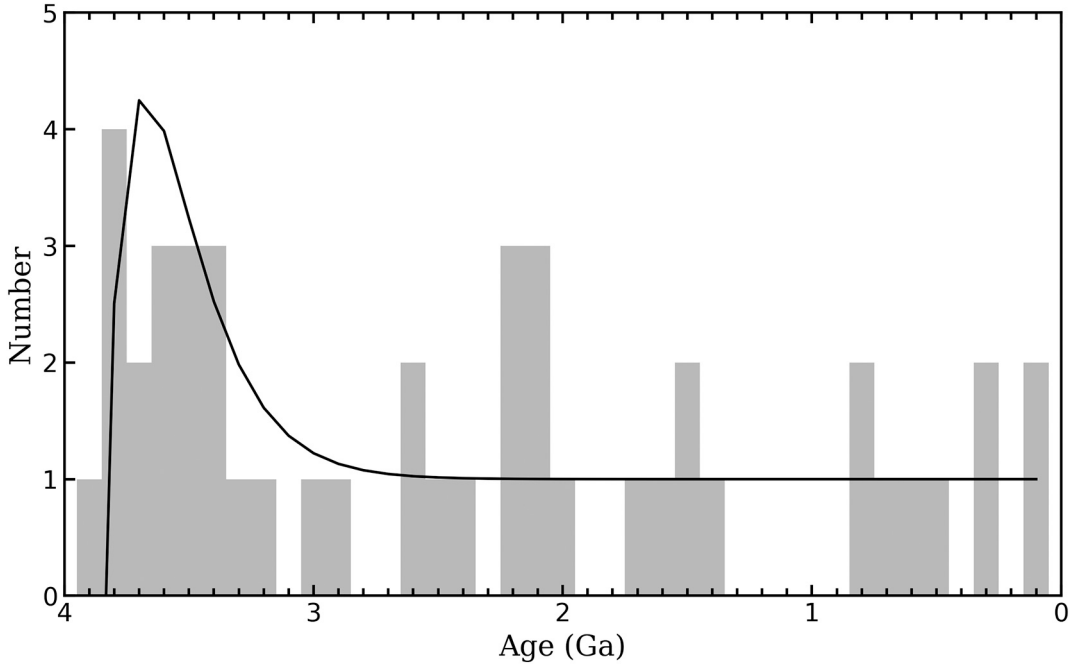

Fig. 5. Illustration of modified chronology function for the second Monte Carlo-type analysis of ages. The modified chronology function is represented by the solid, black line. It is normalized to the number of study craters. The histogram using 0.1 Ga bins of the absolute model (or radiometric for Copernicus and Tycho) ages of all 45 craters are shown by the gray bars.

are erased for surfaces older than ~3.8 Ga, therefore, we would not expect our ages to be accurate beyond this point (e.g., Fassett and Thomson, 2014). The histogram of our estimated ages using 0.1 Ga bins (see Section 3 for reasoning) in Fig. 5 shows that this is indeed the case and verifies our modified chronology. A draw is done 100 times for each observed distribution of ages we analyze (e.g., five crater ages are drawn 100 times for D ≥ 100 km craters). The results of the 100 individual tests are then compared to the observed distribution of ages for *only* ≤ 3 Ga to determine how many times that distribution is observed for a constant distribution. We again assume all sizes have an equal probability of forming. If an observed age distribution is frequently selected (> 5% of the time), we conclude it is consistent with a constant flux. However, if the observed distribution is reproduced ≤1% of the time then we suggest it is plausibly not consistent with a constant flux (similar to ≥3σ significance reported for Gaussian distributions). Values in between 1 and 5% are considered possibly not consistent with a constant flux (similar to ≥2σ significance reported for Gaussian distributions). The disadvantage of this analysis is that age uncertainties can no longer be included. However, we only test for deviations in distributions already indicated to not likely be constant by the first analysis that incorporates uncertainties. Furthermore, although this is the only test for D ≥ 100 and 90 km craters, uncertainties play a minor to no role since these have so few craters with ages ≤3 Ga.

3. Results

Table 2 presents the absolute model formation age, related Stoffler epoch, original USGS epoch, relative age (observed cumulative density at D ≥ 1 km), differential slope of the SSC SFD, and qualitative assessment of the MPF fit to the SSC SFD (see Fig. 3 for examples of fit qualities). Craters are listed by diameter group with largest first (see Table 1 for diameters), then by age. Fig. 6 presents histograms of the model ages using 0.1 Ga bins, along with the summed kernel (Gaussian) density functions of the model ages and their uncertainties (dashed lines) for each diameter range. Other larger bin sizes (it would not make sense to use bin sizes smaller than our precision) were not explicitly tested, because the first Monte Carlo-type analysis using the summed kernel density functions implicitly tested this by incorporating the uncertainties on the ages, which would also be the purpose of using larger bins.

The K–S test results from the first Monte Carlo-type analysis of the distributions of crater formation ages and their uncertainties for diameter ranges testable with this technique (D ≥ 50, 60, 70, and 80 km) indicate that the D ≥ 50 km distribution is the only one that is significantly different (≥ 95%) from a constant flux (Fig. 6f, gray dashed line). The D ≥ 80, 70 and 60 km distributions could all be derived from a constant flux (Fig. 6c–e, gray dashed lines).

From the second Monte Carlo-type statistical analysis of the ages, which cannot include uncertainties, for the D > 100, 90, and 50 km distributions (Fig. 6a, b, f), we find that there are some plausible (probability ≥ 99%) and possible (probability 95–98%) spikes and/or lulls for each distribution (Table 3). Note that the age ranges given include the endpoints for spikes, while they exclude the endpoints for lulls. In Fig. 6 we visualize some of the more probable spikes (black highlights) and lulls (arrows).

Starting with the D ≥ 100 km group, we find that all four craters with more certain formation ages in that set form before our time period of interest, 3.0 Ga (Fig. 6a). Tsiolkovskiy is likely Erastosthenian in age (0.8–3.2 Ga) based upon its morphology (Greenhagen et al., 2016; Pasckert et al., 2015) and crater density on the edge of the crater floor that does not seem to be resurfaced (N[≤ 1 km] ~ 2500; Supplemental Fig. S40). Furthermore, crater density on the mare that covers the majority of the floor appears to be Eratosthenian in age (2.7 ± 0.2 Ga), implying the crater does not need to be older than Eratosthenian to be covered in mare. Our reported "formation" age of 2.6 ± 0.6 Ga, derived from a synthesis of the data, indicates a wide range of ages to consider for determining the significance of spikes and lulls in the 0–3 Ga time frame. If Tsiolkovskiy is >3 Gyrs, then we find that there is a plausible lull from 0 to 3 Ga with a > 99% probability (Table 3). If Tsiolkovskiy is 2.6 Ga, then we find a possible lull from 0 to 2.6 Ga with a 98% probability (indicated by the arrow in Fig. 6a). If Tsiolkovskiy is our youngest suggested age (2.0 Ga), then the lull is at a 95% probability. Thus, in summary, there appears to be a significant lull in cratering with no craters forming for D ≥ 100 km craters, and the length and significance

Table 2
Results for each study crater organized by crater diameter (largest first).

Crater	Age	Stoffler	USGS	Cum. Dens.[a]	Diff. Slope	MPF fit[b]
Tsiolkovskiy[c]	2.6 ± 0.6	Eratosthenian	L. Imbrian	2500 ± 2500	−3.80 ± 0.40	Adequate
Langrenus	3.4 ± 0.2	L. Imbrian	Copernican	5500 ± 1500	−4.16 ± 0.05	Good
Pythagoras	3.5 ± 0.2	L. Imbrian	Eratosthenian	3200 ± 1100	−4.66 ± 0.03	Adequate
Hausen	3.6 ± 0.2	L. Imbrian	Eratosthenian	7300 ± 900	−4.27 ± 0.01	Good
Moretus	3.8 ± 0.1	E. Imbrian	Eratosthenian	19,400 ± 2700	−4.18 ± 0.01	Good
Copernicus	0.8	–	Copernican	–	–	–
Vavilov	1.4 ± 0.1	Eratosthenian	Copernican	N/A	−3.83 ± 0.02	Good
Theophilus	3.0 ± 0.6	Eratosthenian	Copernican	6200 ± 2200	−5.08 ± 0.07	Adequate
Robertson	3.7 ± 0.1	L. Imbrian	Copernican	9500 ± 2900	−4.57 ± 0.06	Good
Tycho	0.1	–	Copernican	–	–	–
Hayn	1.7 ± 0.2	Eratosthenian	Copernican	N/A	−4.05 ± 0.02	Adequate
Aristoteles	2.2 ± 0.4	Eratosthenian	Eratosthenian	N/A	−2.91 ± 0.01	Adequate
Geminus	3.2 ± 0.4	Erato/Imb	Eratosthenian	2000 ± 1500	−4.36 ± 0.08	Good
Olcott	3.4 ± 0.3	L. Imbrian	Eratosthenian	3800 ± 1700	−3.39 ± 0.09	Good
Birkeland	3.8 ± 0.1	E. Imbrian	Eratosthenian	15,000 ± 6400	−3.38 ± 0.03	Adequate
Jackson	0.1 ± 0.1	Copernican	Copernican	N/A	−4.15 ± 0.02	Good
King	0.5 ± 0.2	Copernican	Copernican	N/A	−3.60 ± 0.20	Good
Stevinus	0.6 ± 0.1	Copernican	Copernican	1400 ± 1400	−4.16 ± 0.01	Good
Philolaus	0.8 ± 0.1	Copernican	Copernican	N/A	−3.82 ± 0.01	Good
Plutarch	2.1 ± 0.4	Eratosthenian	Eratosthenian	N/A	−2.85 ± 0.01	Adequate
Sharonov	2.2 ± 0.3	Eratosthenian	Copernican	2400 ± 1700	−4.33 ± 0.36	Good
Fabricus	2.2 ± 0.3	Eratosthenian	L. Imbrian	3800 ± 2200	−2.17 ± 0.11	Good
Finsen	3.4 ± 0.1	L. Imbrian	Eratosthenian	3500 ± 2500	−4.61 ± 0.20	Good
Eudoxus	3.5 ± 0.5	L. Imbrian	Copernican	6500 ± 3300	−2.58 ± 0.00	Adequate
Morse	3.5 ± 0.2	L. Imbrian	Eratosthenian	7800 ± 2600	−2.54 ± 0.08	Adequate
Werner	3.6 ± 0.2	L. Imbrian	L. Imbrian	2900 ± 2900	−2.56 ± 0.01	Adequate
O'Day	3.6 ± 0.1	L. Imbrian	Copernican	4100 ± 4100	−3.81 ± 0.44	Adequate
Ohm	0.3 ± 0.1	Copernican	Eratosthenian	N/A	−4.51 ± 0.03	Good
Zucchius	0.7 ± 0.1	Copernican	Copernican	N/A	−4.47 ± 0.05	Good
Kirkwood	2.4 ± 0.3	Eratosthenian	Eratosthenian	4600 ± 4600	−3.32 ± 0.01	Good
Hercules[c]	2.5 ± 0.7	Eratosthenian	Eratosthenian	N/A	−4.48 ± 0.02	Good
Ricco	3.3 ± 0.4	L. Imbrian	Eratosthenian	N/A	−3.32 ± 0.02	Good
Bullaidus	3.7 ± 0.1	L. Imbrian	Eratosthenian	9800 ± 4900	−3.28 ± 0.21	Adequate
Moiseev	3.9 ± 0.1	Nectarian	Eratosthenian	22,100 ± 9900	−4.28 ± 0.20	Adequate
Anaxagoras	0.3 ± 0.1	Copernican	Copernican	N/A	−4.47 ± 0.04	Good
Leuschner	1.5 ± 0.1	Eratosthenian	L. Imbrian	N/A	−3.26 ± 0.02	Good
Maunder	1.5 ± 0.2	Eratosthenian	Eratosthenian	N/A	−3.63 ± 0.01	Adequate
Aristillus	1.6 ± 0.2	Eratosthenian	Copernican	N/A	−3.58 ± 0.01	Good
Hainzel A	2.0 ± 0.3	Eratosthenian	Eratosthenian	N/A	−2.92 ± 0.04	Good
Cavalerius	2.1 ± 0.3	Eratosthenian	Eratosthenian	2000 ± 2000	−5.36 ± 0.35	Good
Carpenter	2.1 ± 0.4	Eratosthenian	Copernican	15,300 ± 10,800	−3.97 ± 0.02	Good
Eratosthenes	2.6 ± 0.4	Eratosthenian	Eratosthenian	4300 ± 3000	−2.17 ± 0.25	Adequate
Scoresby	2.9 ± 0.5	Eratosthenian	Eratosthenian	9000 ± 9000	−2.85 ± 0.01	Adequate
Hamilton	3.8 ± 0.1	E. Imbrian	Eratosthenian	9600 ± 6800	−3.41 ± 0.25	Adequate
Taruntius	3.8 ± 0.1	E. Imbrian	Copernican	11,000 ± 4500	−4.29 ± 0.11	Good

[a] Observed cumulative density for D ≥ 1 km. N/A indicates that no D ≥ 1 km craters were observed.
[b] "Good" implies most or all of the cumulative crater SFD was fit well by the MPF. "Adequate" means only part of the cumulative crater SFD was fit well or the cumulative crater SFD had large uncertainty and fewer points but was fit well by the MPF. These were determined qualitatively.
[c] Craters with covered floors, and thus, highly uncertain formation ages.

of this lull is dependent on the age of Tsiolkovskiy.

Continuing with D ≥ 90 km craters (Fig. 6b), we find that ages are statistically consistent with a constant flux, unless Tsiolkovskiy is >3.0 Gyrs in age. For an "old" Tsiolkovskiy, we find that there is a possible lull, with no craters forming, between 1.4 and 3.0 Ga (Table 3). The possible lull could be longer from either 0.8–3.0 Ga or 0–3 Ga with some, but fewer than expected, craters forming (Table 3). However, with these results dependent on only one crater of highly uncertain age, we suggest these results are inconclusive.

Finally, for the craters with D ≥ 50 km that have ages ≤3 Ga (Fig. 6f), we find multiple probable and possible spikes and lulls (Table 3). This set now includes two craters with uncertain ages – Tsiolkovskiy and Hercules. What is interesting is that their model age estimations vary in similar ways. They both have a span in "best guess" ages from ~2.0–3.2 Ga with a median age ~ 2.6 Ga (Table 2). We tested six end-member permutations of their ages: the median ages of 2.5 and 2.6 Ga (from Table 2), both >3.0 Ga, one >3.0 Ga and one at 2.6 Ga, one >3.0 Ga and one at 2.0 Ga, one at 2.6 Ga and one at 2.0 Ga, and both at 2.0 Ga. For D ≥ 50 km only in Table 3, we then list only those lulls or spikes that occurred in ≥3 permutations and note the number of permutations for each spike or lull. Those with fewer permutations are given in Supplemental Table S2.

The most probable lull in impact flux for D ≥ 50 km craters occurs between 0.8 and 1.4 Ga (indicated by the arrow in Fig. 6f), but it may possibly be longer (Table 3 and Table S2). A lull in this time span is also indicated by the kernel density function of the ages, which includes the model age's uncertainties (dashed line in Fig. 6f), supporting that this lull is indeed likely. The most probable spike contains the six craters that form from 2.1–2.2 Ga (indicated by black bars in Fig. 6f). Longer spikes with more craters centered around the ~2 Ga value are possible, particularly if Hercules' and Tsiolkovskiy's formation ages are consistent with the younger part of our estimated age range (Table 3 and Table S2). The caveat to this spike is that the model ages in this period have relatively large uncertainties as indicated by the kernel density function (dashed line in Fig. 6f). The kernel density function does not appear to significantly increase (or "spike") in this time frame from ~1.8–2.4 Ga. Thus, our confidence in the spike indicated by the modified Monte Carlo-type analysis is lower than that for the indicated lull. It

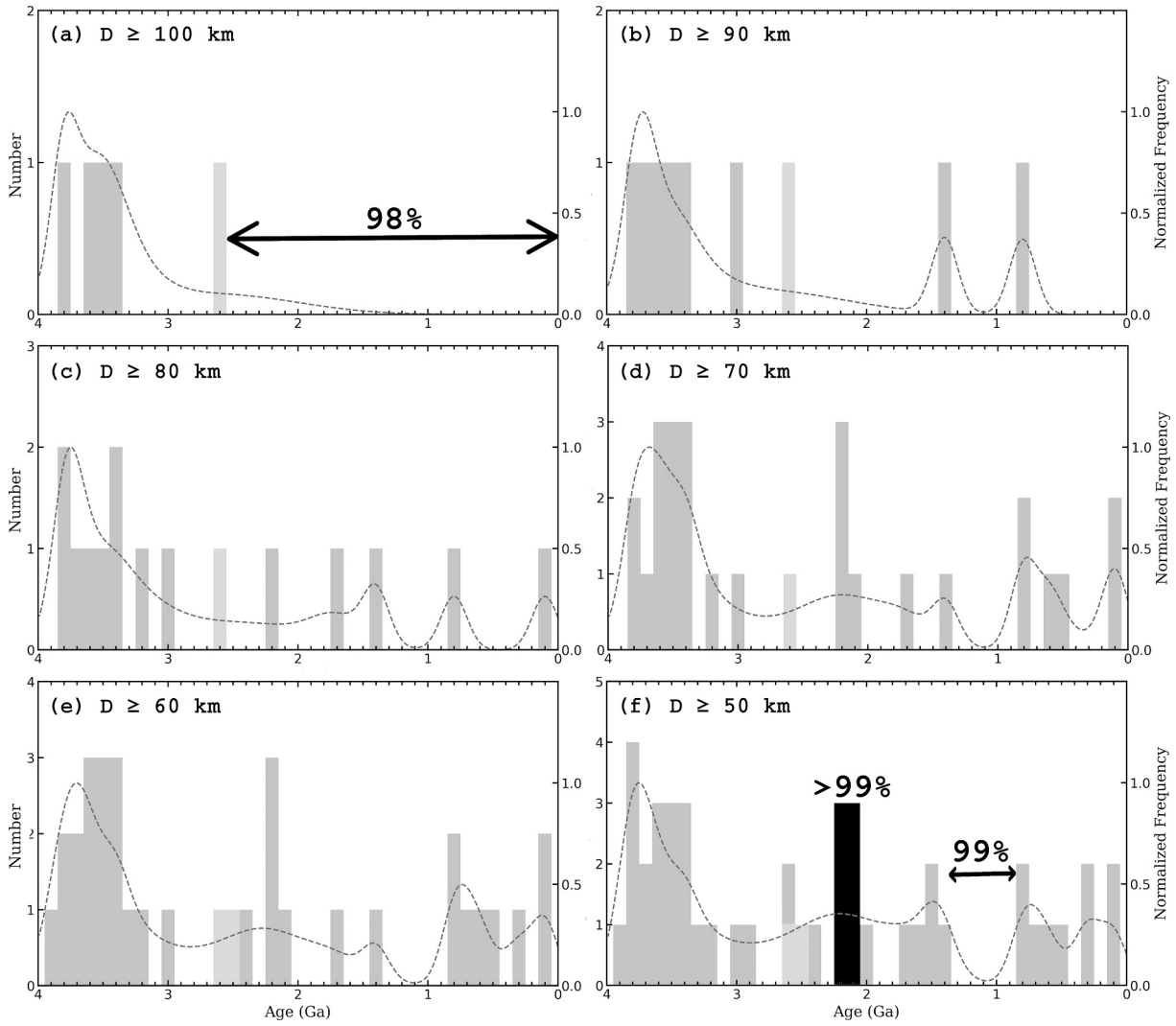

Fig. 6. Histograms of crater ages using 0.1 Ga bins grouped by diameter. The ages of Tsiolkovskiy and Hercules are denoted by lighter gray bars. Significant lulls and a spike found by the second Monte Carlo-type analysis are denoted by arrows and black highlights, respectively. Percentages indicate the significance. A summed kernel density function of the ages and their uncertainties for each diameter range is shown by the dashed line. To produce this function, crater ages and their uncertainties are used as the mean and standard deviation, respectively, of representative Gaussians, which are then summed (see text for further explanation).

could be that most of the difference of the kernel density function for the D ≥ 50 km craters from the constant flux indicated by the K–S test (see above) is in the lull and not the spike.

4. Implications for the Recent Flux of Km-sized impactors

The above results suggesting significant lulls and spikes in the crater model formation ages would tend to support – and be supported by – the other evidence for spikes and lulls observed by different data sets (e.g., Craddock and Howard, 2000; Grieve and Shoemaker, 1994; Hartmann et al., 2007; Mazrouei et al., 2019; Muller et al., 2001; Schmitz et al., 2003), and that at least some of that data may not be biased as previously suggested (e.g., Grier and McEwen, 2001; Huang et al., 2018; Zellner and Delano, 2015). Our work and the other analyses seem to imply the number of impacts may have relatively increased for km-sized impactors for roughly a few hundred million years at around 2 Ga. This is most plausibly produced by formation of an asteroid family or families near strong orbital resonances in the Main Asteroid Belt that would push asteroids into the Earth-Moon system (e.g., Bottke et al., 2007; Nesvorný et al., 2015; Vokrouhlický et al., 2017; Fig. 1). Two intriguing families with possible ages near this time (including error bars) that are also near the 3:1 mean motion resonances with Jupiter – a good resonance for delivering material to the Moon – include Maria (Brož et al., 2013) and New Polana (Bottke et al., 2015; Walsh et al., 2013). However, modeling when these families might produce a surge of impactors is challenging and requires detailed dynamical evolution work (e.g., Bottke et al., 2015).

The suggestion of a continual decrease in the impact flux in the last three billion years (e.g., Hartmann et al., 2007; Lagain et al., 2020) is consistent with our finding of the long-term lull indicated by D ≥ 100 km lunar craters. Our shorter-term lull at ~0.8–1.4 Ga has not been specifically found in any other data set that we know of, but some analyses, such as Mazrouei et al. (2019), indicate short-term lulls at other times, suggesting short-term decreases in impact flux are also plausible. We propose that the lulls occur because either asteroid families do not form at that time or near the strong resonances, as the background rate is likely too low for this size range to provide a constant flux at the levels expected for smaller impactors (e.g., Bottke et al., 2007; Fig. 1). In other words, consider the following. Objects entering resonances along the inner edge of the main belt (e.g., entering the nu6 secular resonance) have a nearly 1–2% probability of striking the Earth, but these probabilities decrease to 0.3%, 0.03%, and 0.01% for the 3:1, 5:2, and 2:1 mean motion resonances with Jupiter at 2.5, 2.8, and 3.3 au, respectively (Bottke et al., 2006). One can obtain impact probability values for

Table 3
Plausible and possible spikes and lulls identified through the second Monte Carlo-type analysis.

Crater set	Spike/ Lull	Probability is spike/Lull	Age range (Ga), # of craters, # of permutations[a]
D ≥ 100 km	Lull	>99%	0.0–3.0, 0
		98%	0.0–2.6, 0
		95%	0.0–2.0, 0
D ≥ 90 km	Lull	96%	1.4–3.0, 0
		96%	0.8–3.0, 1
		95%	0.0–3.0, 2
D ≥ 50 km	Lull	99%	0.8–1.4, 0, 6
		97%	0.8–1.5, 1, 6
		96%	0.8–2.0, 5, 6
			0.8–2.1, 6, 5
		95%	0.3–2.0, 10, 4
			0.3–2.1, 11, 3
	Spike	>99%	2.1–2.2, 6, 6
		99%	2.0–2.1, 7, 3
		98%	2.0–2.6, 11, 3
		96%	2.1–2.4, 7, 6
			2.0–2.4, 8, 3
			2.0–2.5, 9, 3
			1.6–2.2, 10, 3
			1.5–2.2, 11, 5
			1.4–2.2, 12, 4
			1.5–2.6, 15, 3
			1.4–2.6, 16, 3

[a] The number of permutations each spike or lull is observed in is only listed for D ≥ 50 km crater group. Spikes or lulls with < 3 permutation occurrences are listed in Supplemental Table S2.

the Moon by dividing by ~20 (Mazrouei et al., 2019). Thus, all other things being equal, a family forming in the inner main belt near a resonance has a substantial advantage in producing impactors than one that forms in the outer main belt near a resonance. These probabilities naturally imply that most impact surges are associated with family-forming events in the inner and, to a lesser degree, central main belt regions. The exception would be a central or outer main belt family that is so enormous, or that is so strategically located (e.g., located right on the brink of a resonance, so numerous fragments are directly injected into the resonance by the family-forming event), that it is ultimately able to overcome the intrinsic disadvantage of its region. Therefore, if no large asteroids happen to stochastically disrupt near a resonance in then inner or central main belt over some interval, the Earth (and Moon) could see a relative lull in impacts compared to other times. Ideally, future work could use the crater ages on the Moon, and how they wax and wane, to help us interpret the collisional history of the main belt, and vice versa.

Using a very simplified scaling relation, where the crater formed has a diameter 10× the impactor diameter (*d;* e.g., Marchi et al. (2009)), we can try to specify if any variation with diameter has occurred for the Earth-Moon system impact flux in the last 3 Byr. For example, $d \sim$ 5-km impactors form the 50-km craters and $d \sim$ 10-km impactors form the 100-km craters. Consequently, our analysis would imply that the impact flux for ~10-km impactors has been less than expected (Fig. 6a and Table 3) for the constant flux suggested for smaller sub-meter impactors (Marchi et al., 2009; Neukum et al., 2001; Robbins, 2014) that make the smaller, sub-kilometer craters used for model age estimation. This would imply that there are not relatively as many Earth-Moon system impactors ~10 km in diameter for the last 3 Byr. However, as we include "smaller" craters down to D = 60 km, the distribution becomes statistically consistent with a constant flux (Fig. 6b-e), hinting that the $d \gtrsim 6$ km impactors could be apparently produced and reach the Earth-Moon system in the same relative sense with time as the smaller, sub-meter impactors. Nevertheless, our full data set of model formation ages for D ≥ 50 km craters again suggests that a statistically significant lull, and possibly even a spike, occur in the impact flux (Fig. 6f and Table 3). In contrast to the other crater ranges <100 km, this would imply that the $d \gtrsim 5$ km impactor flux would indeed be variable compared with sub-meter impactors. This difference in results for D ≥ 60 km and D ≥ 50 km has two implications: a) the variability in flux for $d \sim$ 5–6 km (and possibly down to roughly several hundred meters; Mazrouei et al., 2019) impactors is so strong that it overwhelms the lack of variability in the $d \sim$ 6–10 km flux; or b) absolute model ages are not yet accurate enough to detect statistically significant spikes and lulls for all crater sizes examined. The former has some support in that smaller impactors should have a higher density than larger impactors (e.g., Bottke et al., 2007; Fig. 1). However, this would require a steeper than expected relative variation in the impactor size-frequency distribution with many more smaller impactors forming, which could have implications for how asteroids break up and the size distribution of the families is generated. Nevertheless, implication (b) is more likely in our opinion, given that uncertainties in absolute model ages are relatively large (Table 2). In addition, the histograms without uncertainties included for the other diameter ranges (Figs. 6b-e) appear to indicate weaker versions of the spike and lull seen for D ≥ 50 in Fig. 6f, if those model ages are their medians.

5. Conclusions

In order to better understand the flux of km-sized asteroids into the Earth-Moon system over the last 3 Ga, we examined the crater retention model ages of D = 50–200 km lunar craters thought to have formed during the Copernican and Eratosthenian (Fig. 2, Tables 1, 2). This initial estimate of crater formation epoch was derived from crater morphologies and superpositions observed using Apollo imaging by the USGS (e.g., Wilhelms and McCauley, 1971) and Wilhelms (1987). Ages in this work are estimated by determining the density of small, superposed craters (diameters between 10s and 100s of meters up to a few kilometers) on the larger crater floors from LROC-WAC and NAC images and then using the Model Production Function (Marchi et al., 2009) (e.g., Figs. 3, 4). We assume that the flux of the small sub-kilometer impactors is exponential for >3 Ga and constant for <3 Ga as proposed by the standard lunar chronologies (e.g., Marchi et al., 2009; Neukum et al., 2001; Robbins, 2014). First, we have found that for some craters our model ages are older than the ages estimated from morphology and superposition (Table 2). For the craters that are still indicated to be ≤3 Ga, we used a Kolmogorov-Smirnov test and Monte Carlo-type analyses to compute the statistical probability that the distribution of ages is not consistent with a constant flux as estimated by standard lunar chronologies for sub-km impactors (e.g., Marchi et al., 2009; Neukum et al., 2001; Robbins, 2014; e.g., Fig. 5). To understand if the flux changes with impactor diameter, we divided the distribution into diameter ranges starting with D ≥ 100 km and decreasing that number by 10 until we got to the minimum of D ≥ 50 km.

We find that the Earth-Moon impact flux may be variable for km-sized impactors. Our most statistically robust results indicate that the impact flux experiences a relative decrease, or "lull", compared to the expected constant flux of sub-kilometer impactors (Fig. 6, Table 3). Furthermore, a less statistically robust result is that a 100–300 Myr relative increase in flux ("spike") may occur ~2 Ga (Fig. 6, Table 3). Our results finding spikes and lulls is consistent with previous work using other datasets, such as radiometric ages of lunar glasses and rock abundance ages of lunar craters (e.g., Craddock and Howard, 2000; Culler et al., 2000; Grieve, 1984; Hartmann et al., 2007; Mazrouei et al., 2019; Schmitz et al., 2003). This potentially contradicts studies that have implied bias in these previous studies (e.g., Huang et al., 2018; Hui et al., 2009) and previous work that have indicated constant fluxes at all impactor diameters (e.g., Grier et al., 2001). However, with the uncertainty in crater retention model ages, we cannot come to any definitive conclusions on possible deviations in bombardment from a constant flux, particularly as it may change with diameter.

It has been proposed that a variation in flux could be caused by formation of asteroid families near strong orbital resonances with the

gas giants in the Main Asteroid Belt (e.g., Bottke et al., 2007; Vokrouhlický et al., 2017; Fig. 1). Our results could support this idea as the possible spike is occurring at a time when some large asteroid families(y) near resonances are suggested to occur (e.g., Bottke et al., 2006; Nesvorný et al., 2015). We further suggest that the possible lulls then occur because either asteroid families are not forming at that time or do not form near resonances that would move asteroids effectively into the Earth-Moon system, since the average background rate may not be high enough to regularly produce impacts (e.g., Bottke et al., 2007; Fig. 1).

Declaration of competing interest

None.

Acknowledgments

This work was supported by NASA's Solar System Exploration Research Virtual Institute (SSERVI) grant NNA14AB03A to the Institute for the Science of Exploration Targets (ISET) node. The authors thank Caleb Fassett and an anonymous reviewer for their detailed comments which helped to improve this manuscript.

Appendix A. Supplementary data

Supplementary data to this article can be found online at https://doi.org/10.1016/j.icarus.2020.114110.

eferences

Baldwin, R.B., 1985. Relative and absolute ages of individual craters and the rate of infalls on the Moon in the post-Imbrium period. Icarus 61, 63–91.
Bierhaus, E.B., McEwen, A.S., Robbins, S.J., Singer, K.N., Dones, L., Kirchoff, M.R., Williams, J.-P., 2018. Secondary craters and ejecta across the solar system: populations and effects on impact-crater based chronologies. Meteorit. Planet. Sci. 53, 638–671. https://doi.org/10.1111/maps.13057.
Bottke, W.F., Vokrouhlický, D., Rubincam, D.P., Nesvorný, D., 2006. The Yarkovsky and YORP effects: implications for asteroid dynamics. Annu. Rev. Earth Planet. Sci. 34, 157–191. https://doi.org/10.1146/annurev.earth.34.031405.125154.
Bottke, W.F., Vokrouhlický, D., Nesvorný, D., 2007. An asteroid breakup 160 Myr ago as the probable source of the K/T impactor. Nature 449, 48–53.
Bottke, W.F., Brož, M., O'Brien, D.P., Campo Bagatin, A., Morbidelli, A., Marchi, S., 2015. The collisional evolution of the main asteroid belt. In: Asteroids IV. Univ. Ariz. Press, pp. 701–724.
Brož, M., Morbidelli, A., Bottke, W.F., Rozehnal, J., Vokrouhlický, D., Nesvorný, D., 2013. Constraining the cometary flux through the asteroid belt during the late heavy bombardment. Astron. Astrophys. 551 https://doi.org/10.1051/0004-6361/201219296. A117.
Craddock, R.A., Howard, A.D., 2000. Simulated degradation of lunar impact craters and a new method for age dating farside mare deposits. J. Geophys. Res. 105, 20387–20401. https://doi.org/10.1029/1999je001099.
Crater Analysis Techniques Working Group, 1979. Standard techniques for presentation and analysis of crater size-frequency data. Icarus 37, 467–474.
Culler, T.S., Becker, T.A., Muller, R.A., Renne, P.R., 2000. Lunar impact history from 40Ar/39Ar dating of glass spherules. Science 287, 1785–1788. https://doi.org/10.1126/science.287.5459.1785.
Fassett, C.I., Thomson, B.J., 2014. Crater degradation on the lunar maria: topographic diffusion and the rate of erosion on the Moon. J. Geophys. Res. Planets 119. https://doi.org/10.1002/2014JE004698, 2014JE004698.
Gladman, B.J., Migliorini, F., Morbidelli, A., Zappala, V., Michel, P., Cellino, A., Froeschle, C., Levison, H.F., Bailey, M., Duncan, M., 1997. Dynamical lifetimes of objects injected into Asteroid Belt resonances. Science 277, 197–201. https://doi.org/10.1126/science.277.5323.197.
Greenhagen, B.T., Neish, C.D., Williams, J.-P., Cahill, J.T.S., Ghent, R.R., Hayne, P.O., Lawrence, S.J., Petro, N.E., Bandfield, J.L., 2016. Origin of the anomalously rocky appearance of Tsiolkovskiy crater. Icarus 273, 237–247. https://doi.org/10.1016/j.icarus.2016.02.041.
Grier, J.A., McEwen, A.S., 2001. The lunar record of recent impact cratering. In: Peucker-Ehrenbrink, B., Schmitz, B. (Eds.), Accretion of Extraterrestrial Matter Throughout Earth's History. Springer US, Boston, MA, pp. 403–422. https://doi.org/10.1007/978-1-4419-8694-8_20.
Grier, J.A., McEwen, A.S., Lucey, P.G., Milazzo, M., Strom, R.G., 2001. Optical maturity of ejecta from large rayed lunar craters. J. Geophys. Res. 106, 32847–32862. https://doi.org/10.1029/1999je001160.
Grieve, R.A.F., 1984. The impact cratering rate in recent time. J. Geophys. Res. Solid Earth 89, B403–B408. https://doi.org/10.1029/JB089iS02p0B403.
Grieve, R.A.F., Shoemaker, E.M., 1994. The record of past impacts on earth. In: Gehrels, T., Matthews, M.S., Schumann, A. (Eds.), Hazards Due to Comets and Asteroids. Univ. Arizona Press, Tucson, pp. 417–462.
Guinness, E.A., Arvidson, R.E., 1977. On the constancy of the lunar cratering flux over the past 3.3×109yr. In: Proc. Lunar Sci. Conf. 8th, pp. 3475–3494.
Hartmann, W.K., 1995. Planetary cratering 1: the question of multiple impactor populations: lunar evidence. Meteoritics 30, 451–467.
Hartmann, W.K., Strom, R.G., Weidenschilling, S.J., Blasius, K.R., Woronow, A., Dence, M.R., Grieve, R.A.F., Diaz, J., Chapman, C.R., Shoemaker, E.M., Jones, K.L., 1981. Chronology of planetary volcanism by comparative studies of planetary cratering. In: Basaltic Volcanism Study Project (Ed.), Basaltic Volcanism on the Terrestrial Planets. Pergamon Press, New York, pp. 1049–1127.
Hartmann, W.K., Quantin, C., Mangold, N., 2007. Possible long-term decline in impact rates: 2. Lunar impact-melt data regarding impact history. Icarus 186, 11–23. https://doi.org/10.1016/j.icarus.2006.09.009.
Hirabayashi, M., Minton, D.A., Fassett, C.I., 2017. An analytical model of crater count equilibrium. Icarus 289, 134–143. https://doi.org/10.1016/j.icarus.2016.12.032.
Huang, Y.-H., Minton, D.A., Zellner, N.E.B., Hirabayashi, M., Richardson, J.E., Fassett, C.I., 2018. No change in the recent lunar impact flux required based on modeling of impact glass spherule age distributions. Geophys. Res. Lett. 45, 6805–6813. https://doi.org/10.1029/2018GL077254.
Hui, S., Norman, M., Jourdan, F., 2009. Tracking formation and transport of Apollo 16 lunar impact glasses through chemistry and dating. In: 9th Australian Space Science Conference, pp. 43–54.
Keller, C.B., Husson, J.M., Mitchell, R.N., Bottke, W.F., Gernon, T.M., Boehnke, P., Bell, E.A., Swanson-Hysell, N.L., Peters, S.E., 2019. Neoproterozoic glacial origin of the Great Unconformity. Proc. Natl. Acad. Sci. 116, 1136. https://doi.org/10.1073/pnas.1804350116.
Kirchoff, M.R., Marchi, S., 2019. The effect of terrain properties on crater model age determination. In: 50th Lunar Planet. Sci. Conf. p. Abst. #2705.
Kirchoff, M.R., Chapman, C.R., Marchi, S., Curtis, K.M., Enke, B., Bottke, W.F., 2013. Ages of large lunar impact craters and implications for bombardment during the Moon's middle age. Icarus 225, 325–341. https://doi.org/10.1016/j.icarus.2013.03.018.
Lagain, A., Bouley, S., Baratoux, D., Costard, F., Wieczorek, M., 2020. Impact cratering rate consistency test from ages of layered ejecta on Mars. Planet. Space Sci. 180, 104755. https://doi.org/10.1016/j.pss.2019.104755.
Le Feuvre, M., Wieczorek, M.A., 2011. Nonuniform cratering of the Moon and a revised crater chronology of the inner solar system. Icarus 214, 1–20. https://doi.org/10.1016/j.icarus.2011.03.010.
Levine, J., Becker, T.A., Muller, R.A., Renne, P.R., 2005. 40Ar/39Ar dating of Apollo 12 impact spherules. Geophys. Res. Lett. 32 https://doi.org/10.1029/2005GL022874. L15201.
Marchi, S., Mottola, S., Cremonese, G., Massironi, M., Martellato, E., 2009. A new chronology for the Moon and Mercury. Astron. J. 137, 4936–4948.
Marchi, S., Massironi, M., Cremonese, G., Martellato, E., Giacomini, L., Prockter, L., 2011. The effects of the target material properties and layering on the crater chronology: the case of Raditladi and Rachmaninoff basins on Mercury. Planet. Space Sci. 59, 1968–1980. https://doi.org/10.1016/j.pss.2011.06.007.
Masiero, J.R., DeMeo, F.E., Kasuga, T., Parker, A.H., 2015. Asteroid family physical properties. In: Asteroids IV. U. Arizona Press, pp. 323–340.
Mazrouei, S., Ghent, R.R., Bottke, W.F., Parker, A.H., Gernon, T.M., 2019. Earth and Moon impact flux increased at the end of the Paleozoic. Science 363, 253. https://doi.org/10.1126/science.aar4058.
McEwen, A.S., Gaddis, L.R., Neukum, G., Hoffman, H., Pieters, C.M., Head, J.W., 1993. Galileo observations of Post-Imbrium lunar craters during the first Earth-Moon flyby. J. Geophys. Res. 98, 17207–17231. https://doi.org/10.1029/93je01137.
Melosh, H.J., 1989. Impact Cratering: A Geologic Process, Oxford Monographs on Geology and Geophysics. Oxford Univ. Press, New York.
Muller, R.A., Becker, T.A., Culler, T.S., Renne, P.R., 2001. Solar system impact rates measured from lunar spherule ages. In: Peucker-Ehrenbrink, B., Schmitz, B. (Eds.), Accretion of Extraterrestrial Matter throughout Earth's History. Springer US, Boston, MA, pp. 447–452. https://doi.org/10.1007/978-1-4419-8694-8_22.
Nesvorný, D., Morbidelli, A., Vokrouhlický, D., Bottke, W.F., Brož, M., 2002. The flora family: a case of the dynamically dispersed collisional swarm? Icarus 157, 155–172. https://doi.org/10.1006/icar.2002.6830.
Nesvorný, D., Vokrouhlický, D., Morbidelli, A., Bottke, W.F., 2009. Asteroidal source of L chondrite meteorites. Icarus 200, 698–701. https://doi.org/10.1016/j.icarus.2008.12.016.
Nesvorný, D., Brož, M., Carruba, V., 2015. Identification and dynamical properties of asteroid families. In: Asteroids IV. U. Arizona Press, pp. 297–321.
Neukum, G., Ivanov, B.A., 1994. Crater size distributions and impact probabilities on Earth from lunar, terrestrial-planet, and asteroid cratering data. In: Gehrels, T., Matthews, M.S., Schumann, A. (Eds.), Hazards Due to Comets and Asteroids. Univ. Arizona Press, Tucson, pp. 359–416.
Neukum, G., Ivanov, B.A., Hartmann, W.K., 2001. Cratering records in the inner solar system in relation to the lunar reference system. Space Sci. Rev. 96, 55–86.
Norman, M.D., Adena, K.J.D., Christy, A.G., 2012. Provenance and Pb isotopic ages of lunar volcanic and impact glasses from the Apollo 17 landing site. Aust. J. Earth Sci. 59, 291–306. https://doi.org/10.1080/08120099.2011.615471.
Oberbeck, V.R., Morrison, R.H., 1974. Laboratory simulation of the herringbone pattern associated with lunar secondary crater chains. The Moon 9, 415–455. https://doi.org/10.1007/bf00562581.
Pasckert, J.H., Hiesinger, H., van der Bogert, C.H., 2015. Small-scale lunar farside volcanism. Icarus 257, 336–354. https://doi.org/10.1016/j.icarus.2015.04.040.

Plescia, J.B., 2012. Uncertainties in the <3 Ga lunar impact cratering chronology. In: 43rd Lunar Planet. Sci. Conf. p. Abst. #1614.
Plescia, J.B., Robinson, M.S., 2011. New constraints on the absolute lunar crater chronology. In: 42nd Lunar Planet. Sci. Conf. p. Abst. #1839.
Robbins, S.J., 2014. New crater calibrations for the lunar crater-age chronology. Earth Planet. Sci. Lett. 403, 188–198. https://doi.org/10.1016/j.epsl.2014.06.038.
Robbins, S.J., Riggs, J.D., Weaver, B.P., Bierhaus, E.B., Chapman, C.R., Kirchoff, M.R., Singer, K.N., Gaddis, L.R., 2018. Revised recommended methods for analyzing crater size-frequency distributions. Meteorit. Planet. Sci. 53, 891–931. https://doi.org/10.1111/maps.12990.
Schmitz, B., Häggström, T., Tassinari, M., 2003. Sediment-dispersed extraterrestrial chromite traces a major asteroid disruption event. Science 300, 961–964. https://doi.org/10.1126/science.1082182.
Stöffler, D., Ryder, G., 2001. Stratigraphy and isotope ages of lunar geologic units: chronological standard for the inner solar system. Space Sci. Rev. 96, 9–54.
Stöffler, D., Ryder, G., Ivanov, B.A., Artemieva, N.A., Cintala, M.J., Grieve, R.A.F., 2006. Cratering history and lunar chronology. Rev. Mineral. Geochem. 60, 519–596. https://doi.org/10.2138/rmg.2006.60.05.
van der Bogert, C., Hiesinger, H., Dundas, C., Krüger, T., McEwen, A., Zanetti, M., Robinson, M., et al., 2017. Origin of discrepancies between crater size-frequency distributions of coeval lunar geologic units via target property contrasts. Icarus 298, 49–63. https://doi.org/10.1016/j.icarus.2016.11.040.
Vokrouhlický, D., Bottke, W.F., Nesvorný, D., 2017. Forming the flora family: implications for the near-earth asteroid population and large terrestrial planet Impactors. Astron. J. 153, 172 (23pp).
Wall, J.V., Jenkins, C.R., 2003. Practical Statistics for Astronomers. Cambridge Univ. Press, Cambridge, UK.
Walsh, K.J., Delbó, M., Bottke, W.F., Vokrouhlický, D., Lauretta, D.S., 2013. Introducing the Eulalia and new Polana asteroid families: re-assessing primitive asteroid families in the inner Main Belt. Icarus 225, 283–297. https://doi.org/10.1016/j.icarus.2013.03.005.
Warner, N.H., Gupta, S., Calef, F., Grindrod, P., Boll, N., Goddard, K., 2015. Minimum effective area for high resolution crater counting of martian terrains. Icarus 245, 198–240. https://doi.org/10.1016/j.icarus.2014.09.024.
Wilhelms, D.E., 1987. The Geologic History of the Moon, U.S. Geol. Surv. Prof. Paper 1348. U.S. Geol. Surv., Washington, DC.
Wilhelms, D.E., McCauley, J.F., 1971. Geological Map of the Near Side of the Moon.
Williams, J.-P., van der Bogert, C.H., Pathare, A.V., Michael, G.G., Kirchoff, M.R., Hiesinger, H., 2017. Dating very young planetary surfaces from crater statistics: a review of issues and challenges. Meteorit. Planet. Sci. 53, 554–582. https://doi.org/10.1111/maps.12924.
Zanetti, M., Stadermann, A., Jolliff, B., Hiesinger, H., van der Bogert, C.H., Plescia, J., 2017. Evidence for self-secondary cratering of Copernican-age continuous ejecta deposits on the Moon. Icarus 298, 64–77. https://doi.org/10.1016/j.icarus.2017.01.030.
Zappalà, V., Cellino, A., Gladman, B.J., Manley, S., Migliorini, F., 1998. Asteroid showers on earth after family breakup events. Icarus 134, 176–179. https://doi.org/10.1006/icar.1998.5946.
Zellner, N.E.B., Delano, J.W., 2015. 40Ar/39Ar ages of lunar impact glasses: relationships among Ar diffusivity, chemical composition, shape, and size. Geochim. Cosmochim. Acta 161, 203–218. https://doi.org/10.1016/j.gca.2015.04.013.
Zellner, N.E.B., Delano, J.W., Swindle, T.D., Barra, F., Olsen, E., Whittet, D.C.B., 2009. Evidence from 40Ar/39Ar ages of lunar impact glasses for an increase in the impact rate ~800 Ma ago. Geochim. Cosmochim. Acta 73, 4590–4597. https://doi.org/10.1016/j.gca.2009.04.027.